The Role of A-Site Ion Nonstoichiometry in the Oxygen Absorption Properties of $Sr_{1+x}Co_{0.8}Fe_{0.2}O_3$ Oxides

Yufeng He

State Key Laboratory of Catalysis, Dalian Institute of Chemical Physics, Chinese Academy of Sciences, Dalian 116023, China; and Graduate School of the Chinese Academy of Sciences, Beijing 100049, China

Xuefeng Zhu and Weishen Yang

State Key Laboratory of Catalysis, Dalian Institute of Chemical Physics, Chinese Academy of Sciences, Dalian 116023, China

$Sr_{1+x}Co_{0.8}Fe_{0.2}O_3$ *($-0.2 \leq$ x ≤ 0.1) oxides have been synthesized and investigated as potential oxygen absorbents for high temperature oxygen separation processes. It was found that the A-site ion deficient* $Sr_{0.95}Co_{0.8}Fe_{0.2}O_3$ *and* $Sr_{0.9}Co_{0.8}Fe_{0.2}O_3$ *oxides have larger oxygen absorption capacities, and slightly higher oxygen desorption rates. However, the A-site ion excess* $Sr_{1.05}Co_{0.8}Fe_{0.2}O_3$ *and* $Sr_{1.1}Co_{0.8}Fe_{0.2}O_3$ *exhibited much higher oxygen desorption rates, but smaller oxygen absorption capacities. The oxygen absorption capacities were further verified using* oxygen temperature-programmed desorption *technique, and the oxygen desorption rates were well described by a pseudo-second-order kinetics model. In addition, the long-term stability of* $Sr_{0.9}Co_{0.8}Fe_{0.2}O_3$ *was investigated for 280 h (1120 loops) with switching between oxygen absorption and desorption. The excellent stability was confirmed by* X-ray diffraction *patterns which suggested that the cyclic processes of oxygen absorption and desorption took place between the perovskite structure with disordered oxygen vacancies and the brownmillerite structure with ordered oxygen vacancies.* © 2010 American Institute of Chemical Engineers *AIChE J,* 57: 87–95, 2011
Keywords: absorbents, oxygen separation, absorption capacity, desorption rate, stability

Introduction

Ceramic materials have been widely studied by many people all over the world because of their numerous applications, including dense oxygen permeation membranes for air separation, catalysts for hydrocarbon oxidation, cathode materials for solid oxide fuel cells, oxygen sensors, and absorbents.[1–6] In particular, the perovskite-type dense ceramic membranes made of mixed ionic and electronic conducting oxides have received considerable attention over the past two decades for oxygen separation from air and as membrane reactors for light hydrocarbon conversion to valuable products.[7–10] However, the research into the use of perovskite-type complex oxides as oxygen absorbents for oxygen separation began only in 2000.[11] Lin's group[12] first reported that perovskite-type absorbent materials with variable oxygen contents had important characteristics, including an infinite selectivity to O_2 over N_2 or other gases, a high oxygen absorption rate and a large oxygen absorption capacity. All of these characteristics might overcome the selectivity and stability drawbacks found in zeolite absorbents. It has been reported that perovskite-type oxides could be

used for oxygen enrichment by temperature swing absorption.[13] Karppinen et al.[14–16] have systemically studied the oxygen absorption/desorption properties of $RBaCo_4O_{7+\delta}$ (R = Y, Dy, Ho, Er, Tm, Yb, and Lu), in particular the compound $YBaCo_4O_{7+\delta}$, by a Thermogravimetric Analysis (TGA) technique. They discovered that $RBaCo_4O_{7+\delta}$ could absorb and desorb a large amount of oxygen over a narrow temperature range (200–400°C), and the absorption and desorption processes were highly reversible. Guntuka et al.[17,18] investigated the oxygen absorption and desorption characteristics of A- and B-site substituted lanthanum cobaltite perovskite-type oxides. They found that, among the oxides studied, $SrCo_{0.5}Fe_{0.5}O_{3-\delta}$ and $La_{0.1}Sr_{0.8}Ag_{0.1}Co_{0.5}Fe_{0.5}O_{3-\delta}$ were the preferred absorbent materials by virtue of their optimum equilibrium absorption capacities and sorption–desorption kinetics. In our laboratory, we have investigated the impact of A-site substitution on the oxygen absorption and desorption properties of $Ba_{1-x}Sr_xCo_{0.5}Fe_{0.5}O_{3-\delta}$ ($0 \leq x \leq 1$) oxides, and have applied the oxygen absorption process to a membrane separation program.[19,20]

The effects of dopant species and dopant concentrations on the properties of perovskite-type ceramic materials used as oxygen permeation membranes and oxygen absorbents have been extensively studied. In addition, the impact of defects, for instance the deviation of the A/B ratio from unity, on the characteristics of oxygen permeation and oxygen absorption/desorption may be very important. The use of A-site deficient or excess Fe–Co based perovskite oxides as cathodes for Solid Oxide Fuel Cells (SOFCs) and oxygen permeation membranes for air separation have been reported.[21–23] As described by Poulsen,[24] the deviation of A/B from unity can lead to the formation of oxygen vacancies and thus enhance the oxygen ionic conductivity. Waller et al.[25] found that the decrease of electrode resistance resulted from the preferential formation of oxygen vacancies for perovskite-type electrodes with an A-site ion deficiency. When A-site ions were deficient, a remarkable decrease in Area Specific Resistance (ASR) was also discovered for $(La_{0.6}Sr_{0.4})_{1-s}Co_{0.2}Fe_{0.8}O_{3-\delta}$ perovskites, and the highest electro-catalytic activity for the reduction of oxygen was achieved with the oxide $(La_{0.6}Sr_{0.4})_{0.85}Co_{0.2}Fe_{0.8}O_{3-\delta}$, with an ASR of 14.8 Ω cm^2 at 600°C.[22] In addition, in 1996, Kharton's group found that the creation of vacancies in the A- or B-site sublattices of $Sr_{0.65}La_{0.35}CoO_{3-\delta}$ perovskite oxide resulted in a reduction of oxygen permeation fluxes; the ionic deficiency on the B-site had smaller influence on the oxygen permeability compared with that on the A-site.[9] Recently, Shao's group studied the properties of A/B-site ion deficient $(Ba_{0.5}Sr_{0.5})_{1-x}(Co_{0.8}Fe_{0.2})_yO_{3-\delta}$ (x = 0–0.3) ($0.77 \leq y \leq 1.00$) oxides as oxygen permeation membranes, and also investigated A-site ion excess $(Ba_{0.5}Sr_{0.5})_{1+x}Co_{0.8}Fe_{0.2}O_{3-\delta}$ ($0 \leq x \leq 0.3$) compounds as cathodes for SOFCs.[26–28] The highest oxygen permeability was recorded for $(Ba_{0.5}Sr_{0.5})_{1-x}Co_{0.8}Fe_{0.2}O_{3-\delta}$ (x = 0.03) at 900°C, with the permeation flux reaching about 3.5×10^{-6} mol cm^{-2} s^{-1} (STP) for the 1 mm thick membrane, as compared with 2.5×10^{-6} mol cm^{-2} s^{-1} (STP) for the $(Ba_{0.5}Sr_{0.5})_{1-x}Co_{0.8}Fe_{0.2}O_{3-\delta}$ (x = 0.0) membrane under the same conditions. For $(Ba_{0.5}Sr_{0.5})(Co_{0.8}Fe_{0.2})_yO_{3-\delta}$ ($0.77 \leq y \leq 1.00$) membranes, the formation of an appropriate concentration of B-site ion deficiency has greatly restrained the A-

site ion diffusion, and thus stabilized the perovskite structure and consequently the oxygen permeation flux. The excess of A-site ions for $(Ba_{0.5}Sr_{0.5})_{1+x}Co_{0.8}Fe_{0.2}O_{3-\delta}$ ($0 \leq x \leq 0.3$) cathode materials resulted in expansion of cell volumes and decrease of electronic conductivities. However, the polarization resistance of the oxygen reduction process was reduced significantly for the oxide with an appropriate A-site ion excess, for instance, $(Ba_{0.5}Sr_{0.5})_{1.03}Co_{0.8}Fe_{0.2}O_{3-\delta}$, due to the formation of more oxygen vacancies and more active sites.

The present work was aimed at studying the influences of A-site ionic deficiency and excess on the oxygen absorption/desorption properties of $Sr_{1+x}Co_{0.8}Fe_{0.2}O_{3-\delta}$ ($-0.2 \leq x \leq 0.1$) compounds, with particular reference to the oxygen desorption rates. In addition, the long-term stability of the oxygen absorption/desorption processes was examined.

Experimental

Preparation of materials

Powder samples of $Sr_{1+x}Co_{0.8}Fe_{0.2}O_{3-\delta}$ ($-0.2 \leq x \leq 0.1$) oxides were prepared by a combined Ethylene Diamine Tetra-acetic Acid (EDTA)–citric acid complexing method.[29] The concentrations of metal nitrate solutions were determined by titration. During a synthetic process, the calculated amounts of $Sr(NO_3)_2$ ($\geq 99.5\%$), $Co(NO_3)_2 \cdot 6H_2O$ ($\geq 99.0\%$), $Fe(NO_3)_3 \cdot 9H_2O$ ($\geq 98.5\%$) were added to a beaker, followed by EDTA and citric acid. The mole ratio of EDTA, citric acid, and total metal ions was about 1:1:1. $NH_3 H_2O$ was used to adjust the solution pH value to around 6, at which point the solution immediately became transparent. After the polymerization and condensation reactions had taken place, a dark purple gel was obtained. Then, the as-prepared gel was reheated till self-ignition took place, giving a primary powder with the desired stoichiometry. Finally, the green powder was calcined in air at 900°C for 5 h. After these procedures, some of the resulting powder was pressed and then crushed into 20–40 mesh granules for the stable state oxygen absorption experiment and oxygen temperature-programmed desorption (O_2-TPD) testing, and some $Sr_{0.9}Co_{0.8}Fe_{0.2}O_3$ powder was pressed into the pellet with a diameter of 13 mm and a thickness of 1.2 mm for high temperature in-situ X-ray diffraction (XRD).

It is well known that simple metal oxide catalysts (such as manganese oxide, iron oxide, and cobalt oxide) show good catalytic reduction abilities for oxygen.[30] In our laboratory, Co_3O_4 with high oxygen reduction activity reduced cathode polarization resistance, and consequently improved performances of solid oxide full cells, when the oxide was mixed with cathodes.[5] And in this article, the Co_3O_4 phase appeared in $Sr_{1+x}Co_{0.8}Fe_{0.2}O_3$ (x = –0.1, –0.2) oxides. Thereby, the influences of Co_3O_4 on the oxygen absorption and desorption properties of $SrCo_{0.8}Fe_{0.2}O_3$ absorbent were tested. The Co_3O_4 oxide was also synthesized by the combined EDTA–citric acid complexing method as described above. The resulting powder was mixed with $SrCo_{0.8}Fe_{0.2}O_3$ with different ratios by weight. After grinding in ethanol for about an hour, the mixtures were pressed and crushed into 20–40 mesh granules for stable state oxygen absorption experiments.

Characterization of materials

The crystal structures of the synthesized powder samples were checked by XRD (Rigaku D/Max-RB, Cu Kα radiation) in the 2θ range of 20–80° with a step width of 0.02°.

A high temperature in situ XRD technique was used for monitoring the phase changes of the oxide by the same diffractometer as above, so as to fully understand oxygen absorption and desorption mechanisms. For the measurement, the 2θ range was 30–50° with a scanning rate of 10°/min and a sampling interval of 1 min. The operating temperature was kept at 500°C. The fluxes of synthesized air and nitrogen were both about 30 ml/min, with synthesized air for oxygen absorption process and nitrogen for oxygen desorption process.

The oxygen desorption properties of the defect perovskite-type oxides were investigated by the O_2-TPD measurement. About 0.60 g of each sample was packed into a Φ 6 (mm) quartz tube. Helium was used as the carrier gas with a flow rate of 40 ml/min. The temperature was increased from 100°C to 950°C at a rate of 10°C/min. A Thermal Conductivity Detector (TCD) was equipped for signal detection along with a computer data acquisition system.

Oxygen absorption and desorption of materials

Oxygen absorption experiments were performed on a fixed-bed oxygen absorption apparatus, as shown in Ref. 19, which consisted of a gas delivery system, a temperature control system, an oxygen absorption column, an oxygen sensor (GPR-3100, Advanced Instruments) and a computer for data storage. During measurements, the oxygen concentrations in the effluent gases from the absorption column were continuously monitored by the oxygen sensor. Data collection and storage were performed simultaneously by the computer. The operating temperatures for all samples were in the range of 450–600°C. The oxygen absorption and desorption processes were carried out at ambient pressure. Synthesized air (P_{O2}, 0.21 atm) and high purity helium (P_{O2}, 10^{-5} atm), were used for oxygen absorption and absorbent regeneration, respectively. During all the oxygen absorption and desorption experiments, the air and helium fluxes were kept at about 50 and 100 ml/min, respectively. The oxygen absorption capacities were all corrected for dead-volume times.

Stability testing of oxygen absorption and desorption cycles was carried out on the equipment based on that described elsewhere[19,20] and shown in Figure 1. Two fixed-bed absorption beds were used for the cyclic testing, with one for the oxygen absorption and the other for the oxygen desorption by turn. Two identical quartz tubes filled with 19 g of $Sr_{0.9}Co_{0.8}Fe_{0.2}O_{3-\delta}$ acted as the oxygen absorption beds. The outflow from the oxygen absorption tube was connected to a gas chromatograph, while that from the oxygen desorption tube was analyzed by the oxygen sensor. At first, the stability experiment was operated at $T = 500°C$, with an interval of 15 min, an air flux of 48.15 ml/min and helium flux of 325 ml/min. To obtain a larger oxygen absorption capacity with the lowest oxygen mole fraction in the effluent from the oxygen absorption bed, or to get a better oxygen absorption efficiency for the absorbent, the temperature for
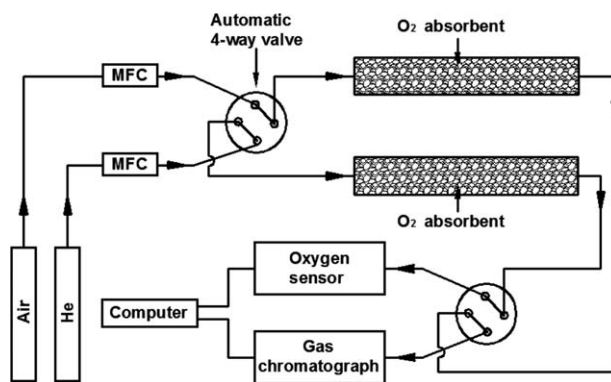

Figure 1. Schematic diagram of the oxygen absorption setup for long-term stability operation.

MFC, mass flow controller.

the stability experiment was raised to 550°C, with the same interval time of 15 min, the air flux of 54.69 ml/min and helium flux of 370 ml/min. As reported by Zhu et al.,[20] the high purity helium or other inert gas was usually used as the purging gas to regenerate the absorbent on the laboratory scale, to simplify the operating system. However, on a larger scale for industrial production, a vacuum pump can be used to renew the saturated oxygen absorbent, giving a true pressure swing absorption (PSA) process just like the PSA of zeolites. In this way, the high purity oxygen and pure nitrogen can be collected together.

Results and Discussion

Figure 2 shows the XRD patterns of the $Sr_{1+x}Co_{0.8}Fe_{0.2}O_3$ ($-0.2 \leq x \leq 0.1$) oxides at room temperature. It indicates that the samples with compositions $-0.05 \leq x \leq 0.05$ have single phase cubic perovskite structure. For $Sr_{0.8}Co_{0.8}Fe_{0.2}O_3$ and $Sr_{0.9}Co_{0.8}Fe_{0.2}O_3$ oxides with A-site deficiency, $x = -0.2, -0.1$, the main diffraction peaks are those of the cubic perovskite phase, except that some diffraction peaks of Co_3O_4/CoO (Fe_3O_4/FeO) appear. Furthermore, the intensity of CoO_x (FeO_x) in $Sr_{0.8}Co_{0.8}Fe_{0.2}O_3$ is stronger than that in $Sr_{0.9}Co_{0.8}Fe_{0.2}O_3$. For the $Sr_{1.1}Co_{0.8}Fe_{0.2}O_3$ compound with A-site ionic excess, the diffraction pattern mostly displays the cubic perovskite structure, with some peaks of an unknown phase. As reported in Ref. 28 the upper limit of the A-site ion excess was around 9 mol% among the $(Ba_{0.5}Sr_{0.5})_{1+x}Co_{0.8}Fe_{0.2}O_{3-\delta}$ ($0 \leq x \leq 0.3$) oxides, with retaining the pure phase perovskite structure. In this work, for the series of $Sr_{1+x}Co_{0.8}Fe_{0.2}O_3$ ($-0.2 \leq x \leq 0.1$) oxides, the A-site ion deficiency or excess needs to be kept in the range $-0.05 \leq x \leq 0.05$ (5 mol%) to synthesize single phase cubic perovskite oxides.

For the $Sr_{1+x}Co_{0.8}Fe_{0.2}O_{3-\delta}$ ($-0.2 \leq x \leq 0.1$) samples, oxygen partial PSA experiments were performed in the temperature range of 450–600°C. At each temperature, the equilibrium oxygen absorption and desorption processes were carried out. The results, giving oxygen absorption capacities, are shown in Figure 3. The oxygen absorption capacities were calculated using the published equation.[19]
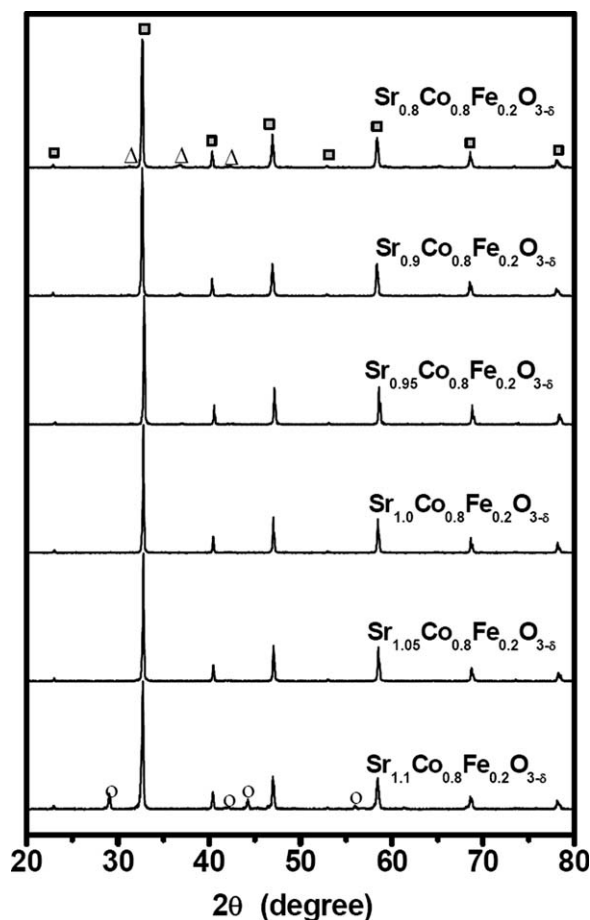
Figure 2. Room temperature XRD patterns of the $Sr_{1+x}Co_{0.8}Fe_{0.2}O_{3-\delta}$ ($-0.2 \leq x \leq 0.1$) oxides.

□: cubic perovskite phase, △: CoO_x (FeO_x) phases, ○: unknown phase.

$$q_{abs} = \frac{F_{air}}{m} \int_0^t \left(\frac{x_{in} - x_{out}}{1 - x_{out}} \right) dt \qquad (1)$$

where q_{abs} is the oxygen absorption capacity, F_{air} is the flux of the synthesized air, t and m are the oxygen absorption time and the weight of the oxide absorbent, and x_{in} and x_{out} are the oxygen mole fractions in the feed air and effluent, respectively, during an oxygen absorption measurement. The plots in Figures 3a, b both indicate that the $Sr_{1+x}Co_{0.8}Fe_{0.2}O_3$ oxide with $x = -0.05$ has the largest oxygen absorption capacity. In other words, the materials $Sr_{0.95}Co_{0.8}Fe_{0.2}O_3$ and $Sr_{0.9}Co_{0.8}Fe_{0.2}O_3$ with A-site deficiency both exhibit larger oxygen absorption capacities than that of $SrCo_{0.8}Fe_{0.2}O_3$ with A-site ion stoichiometry, at both 500 and 550°C. As Shao's group reported, the creation of a particular A-site ion deficiency in $(Ba_{0.5}Sr_{0.5})_{1-x}Co_{0.8}Fe_{0.2}O_3$ ($x = 0-0.3$), for example $(Ba_{0.5}Sr_{0.5})_{0.97}Co_{0.8}Fe_{0.2}O_3$, not only can result in an increase of oxygen vacancy concentration but also can enhance the average oxidation states of Co^{3+} (Fe^{3+}) to Co^{4+} (Fe^{4+}), and so more α-oxygen can be absorbed or desorbed in the relatively low temperature range of 450–600°C in the O_2-TPD experiment.[26]

Hence, A-site ion deficiency in $Sr_{0.95}Co_{0.8}Fe_{0.2}O_3$ and $Sr_{0.9}Co_{0.8}Fe_{0.2}O_3$ oxides may lead to higher average oxidation states of B-site ions (Co and Fe), as well as more oxygen vacancies. However, the oxygen absorption capacities of another three A-site ion non-stoichiometric oxides $Sr_{0.8}Co_{0.8}Fe_{0.2}O_3$, $Sr_{1.05}Co_{0.8}Fe_{0.2}O_3$ and $Sr_{1.1}Co_{0.8}Fe_{0.2}O_3$ are smaller than that of $SrCo_{0.8}Fe_{0.2}O_3$. As mentioned above, the decreases of oxygen absorption capacities of $Sr_{1+x}Co_{0.8}Fe_{0.2}O_3$ ($x = -0.2, 0.05, 0.1$) oxides are because the average oxidation states of the B-site ions (Co and Fe) are reduced owing to the deficiency or excess of A-site ions, and not because other minority phases appear for $Sr_{0.8}Co_{0.8}Fe_{0.2}O_3$ and $Sr_{1.1}Co_{0.8}Fe_{0.2}O_3$ oxides. It also indicates that, for these three A-site ion deficient or excess $Sr_{1+x}Co_{0.8}Fe_{0.2}O_3$ ($x = -0.2, 0.05, 0.1$) oxides with smaller oxygen absorption capacities, the charge compensation mechanism is achieved through the formation of more oxygen vacancies and the reduction of the average oxidation states of Co (Fe), which can be further confirmed by the amounts of α-oxygen desorbed in the low temperature range of the latter O_2-TPD experiment. Note that, for the A-site ion nonstoichiometric $Sr_{1+x}Co_{0.8}Fe_{0.2}O_3$ ($x = -0.2, 0.05, 0.1$) oxides, the less amount of α-oxygen the oxide desorbs in the low temperature range of 300–600°C, the lower the average oxidation state of its B-site ions is, and correspondingly the higher oxygen vacancy
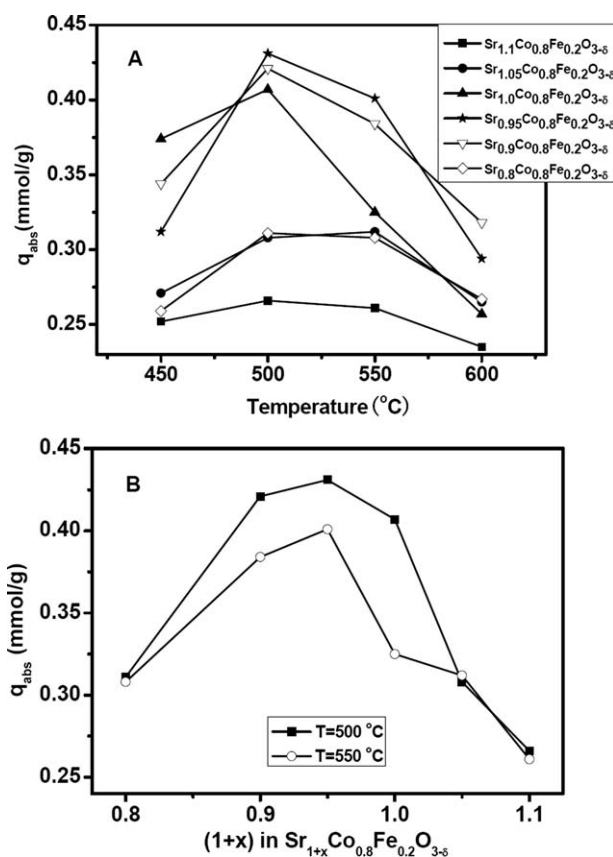

Figure 3. (A) Oxygen absorption capacities of the $Sr_{1+x}Co_{0.8}Fe_{0.2}O_{3-\delta}$ ($-0.2 \leq x \leq 0.1$) oxides in the temperature range of 450–600°C. (B) Dependence of oxygen absorption capacities on Sr concentrations of the $Sr_{1+x}Co_{0.8}Fe_{0.2}O_{3-\delta}$ oxides at 500 and 550°C.

Table 1. Data of the Fixed-Bed Oxygen Absorption Capacities and Modeling Oxygen Desorption Rates of the $Sr_{1+x}Co_{0.8}Fe_{0.2}O_{3-\delta}$ ($-0.2 \leq x \leq 0.1$) Oxides at 500°C

	q_{abs} (mmol/g)	k'_{des} [g/(mmol min)]	R'^2	S
$Sr_{1.1}Co_{0.8}Fe_{0.2}O_3$	0.266	1.41	0.998	479
$Sr_{1.05}Co_{0.8}Fe_{0.2}O_3$	0.308	1.14	0.998	713
$Sr_{1.0}Co_{0.8}Fe_{0.2}O_3$	0.407	0.156	0.974	744
$Sr_{0.95}Co_{0.8}Fe_{0.2}O_3$	0.431	0.248	0.977	806
$Sr_{0.9}Co_{0.8}Fe_{0.2}O_3$	0.419	0.501	0.990	755
$Sr_{0.8}Co_{0.8}Fe_{0.2}O_3$	0.311	0.645	0.997	705

q_{abs} is the fixed-bed oxygen absorption capacity, k'_{des} the oxygen desorption rate coefficient, R'^2 the desorption rate correlation coefficient, and S the integral area of the α-oxygen peak within the low temperature range (300–600°C) of the O2-TPD curve.

Figure 4. Oxygen desorption kinetic curves of $Sr_{1+x}Co_{0.8}Fe_{0.2}O_{3-\delta}$ ($-0.2 \leq x \leq 0.1$) at 500°C.

1,1′. $Sr_{1.1}Co_{0.8}Fe_{0.2}O_{3-\delta}$, 2,2′. $Sr_{1.05}Co_{0.8}Fe_{0.2}O_{3-\delta}$, 3,3′. $Sr_{1.0}Co_{0.8}Fe_{0.2}O_{3-\delta}$, 4,4′. $Sr_{0.95}Co_{0.8}Fe_{0.2}O_{3-\delta}$, 5,5′. $Sr_{0.9}Co_{0.8}Fe_{0.2}O_{3-\delta}$, 6,6′. $Sr_{0.8}Co_{0.8}Fe_{0.2}O_{3-\delta}$. 1, 2, 3, 4, 5, 6 are the modeling kinetic plots of the experimental data; 1′, 2′ 3′, 4′, 5′, 6′ are the straight lines deduced from the modeling kinetic plots.

concentration the oxide has, with the charge compensation mechanism controlling. Therefore, the three oxides with lower average oxidation states of B-site ions (or less amount of α-oxygen) have smaller oxygen absorption capacities. In addition, the oxygen absorption capacities of the $Sr_{1+x}Co_{0.8}Fe_{0.2}O_{3-\delta}$ ($-0.2 \leq x \leq 0.1$) oxides at $T = 500$°C are listed in the first column of Table 1, and the relative peak areas of α-oxygen desorbed in the low temperature range (300–600°C) in the latter TPD experiment are shown in the last column of Table 1.

Defect perovskite-type oxygen absorbents usually show much higher oxygen absorption rates than desorption ones, which has been verified before.[19,31] Therefore, besides the oxygen absorption capacity, the oxygen desorption rate should be investigated seriously. The oxygen desorption processes of the six oxides $Sr_{1+x}Co_{0.8}Fe_{0.2}O_3$ ($-0.2 \leq x \leq 0.1$) are modeled using the pseudo-second-order kinetics as described elsewhere.[32,19] The model presumes that the oxygen desorption is complete ($x_{O2} \approx 0$) when the oxygen mole fraction x_{O2} in the effluent exiting from the quartz tube is about 0.005 during a desorption process.

$$\frac{dq_{des}}{dt} = k'_{des}(q'_{eq} - q_t)^2 \qquad (2)$$

The integrated linear equation, known as the Lagergren equation, is

$$\frac{t}{q_t} = \frac{1}{k'_{des}q'^2_{eq}} + \frac{1}{q'_{eq}}t \qquad (3)$$

where q'_{eq} and q_t are the amounts of oxygen desorbed in equilibrium with the surrounding atmosphere and at time t, and k'_{des} is the rate coefficient for the oxygen desorption processes. The modeling lines of the fixed-bed oxygen desorption processes and the straight lines deduced from the modeling lines are shown in Figure 4. The slopes and intercepts of the straight lines are used to calculate the oxygen desorption rate coefficients k'_{des}, which are shown in Table 1. The patterns in Figure 4 and the correlation coefficients R'^2 in Table 1 indicate that the experimental data fit well with the pseudo-second-order kinetics equations. The most important factor is that the values of k'_{des} in Table 1 suggest that the deficiency or excess of A-site ions can accelerate the oxygen desorption from its corresponding oxide. Among the series of A-site ion deficient
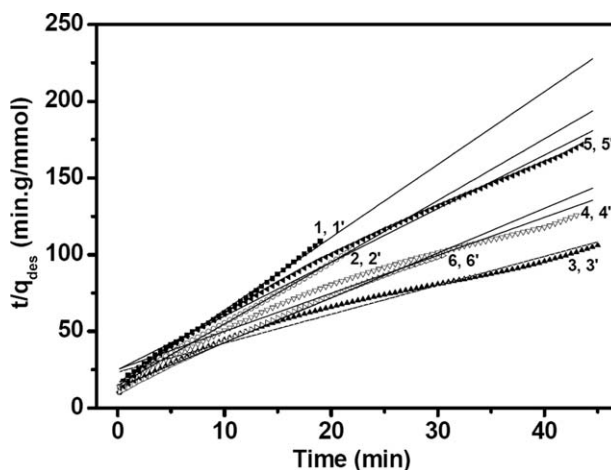
$Sr_{1+x}Co_{0.8}Fe_{0.2}O_3$ ($-0.2 \leq x < 0$) oxides, the larger the nonstoichiometry value x is, the higher the oxygen desorption rate is. Since oxygen absorption into and desorption from the small absorbent granules are limited by oxygen surface-exchange processes,[19] the higher rate makes clear that the charge compensation mechanism, as a result of the A-site ion deficiency, results in more oxygen vacancies emerging in the absorbent granules, and so more active sites appearing on their surface. In addition to the greater number of oxygen vacancies, some CoO_x (FeO_x) impurities can also enhance the oxygen desorption rates of $Sr_{0.8}Co_{0.8}Fe_{0.2}O_3$ and $Sr_{0.9}Co_{0.8}Fe_{0.2}O_3$ oxides.

The oxygen absorption and desorption properties of $SrCo_{0.8}Fe_{0.2}O_3$ oxide with different Co_3O_4 concentrations are tested in the paper. It has been confirmed that Co_3O_4 does not absorb or desorb oxygen below 760°C, because the reaction $Co_3O_4 \Leftrightarrow 3CoO + \frac{1}{2}O_2$ occurs only above 760°C.[33] Therefore, the component for oxygen absorption is the perovskite oxide $SrCo_{0.8}Fe_{0.2}O_3$, and Co_3O_4 just acts as a kind of catalyst for oxygen absorption and desorption. As shown in the last column of Table 2, the presence of Co_3O_4 in all

Table 2. Data of the Fixed-Bed Oxygen Absorption Capacities and Modeling Oxygen Desorption Rates of the $SrCo_{0.8}Fe_{0.2}O_{3-\delta}$ Oxide Mixed with Different Co_3O_4 Concentrations at 500°C

$x\%$ ($Co_3O_4\%$)	q_{abs} (mmol/g)	$q_{abs}/(1-x\%)$ (mmol/g)	k'_{des} [g/(mmol min)]
0%	0.407	0.407	0.152
5%	0.372	0.392	0.200
10%	0.366	0.407	0.371
20%	0.293	0.366	0.935
30%	0.250	0.357	0.902

$x\%$ is the weight ratio of Co_3O_4 in an absorbent mixture, q_{abs} the fixed-bed oxygen absorption capacity, $q_{abs}/(1-x\%)$ the real oxygen absorption capacity of $SrCo_{0.8}Fe_{0.2}O_3$, and k'_{des} the oxygen desorption rate coefficient.

mixtures speeds the oxygen desorption from $SrCo_{0.8}Fe_{0.2}O_3$. Within the composition range $5\% \leq Co_3O_4\%$ (wt %) $\leq 20\%$, the greater the amount of Co_3O_4 is, the higher the oxygen desorption rate is. Note that the desorption rate of the absorbent with 30% Co_3O_4 is a little lower than that with 20% Co_3O_4. The data in the second column indicate that Co_3O_4 does not affect the oxygen absorption capacity of $SrCo_{0.8}Fe_{0.2}O_3$ when the concentration of Co_3O_4 is less than 20%. In conclusion, in order to optimize the oxygen absorption and desorption properties, the concentration of Co_3O_4 in the mixture should be 20% (wt %).

For $Sr_{1.05}Co_{0.8}Fe_{0.2}O_3$ and $Sr_{1.1}Co_{0.8}Fe_{0.2}O_3$ oxides, the excesses of A-site ions both resulted in higher oxygen desorption rates, due to the formation of more oxygen vacancies and so more active sites for oxygen desorption and absorption. Evidence for this is provided by the values of $3-\delta$ for $(Ba_{0.5}Sr_{0.5})_{1+x}Co_{0.8}Fe_{0.2}O_{3-\delta}$ with $0 \leq x \leq 0.20$,[28] although there is some impurity appearing for the $Sr_{1.1}Co_{0.8}Fe_{0.2}O_3$ oxide. Because oxygen absorption and desorption are limited by oxygen surface-exchange processes,[19] so the impurity could block the active sites on the small absorbent granule surface for oxygen absorption and desorption, but the result of the competition between the formation of more active sites and fewer active sites blocked by the impurity eventually accelerates the oxygen desorption from $Sr_{1.1}Co_{0.8}Fe_{0.2}O_3$. In addition, for $Sr_{1+x}Co_{0.8}Fe_{0.2}O_3$ ($0 \leq x \leq 0.1$) oxides, the increase of oxygen vacancy concentrations can be confirmed by the reduction of the amounts of α-oxygen desorbed in the low temperature range in the latter O_2-TPD experiment, owing to the A-site ion excess.

For defect perovskite-type oxides, the oxygen desorption characteristics are usually studied by the O_2-TPD technique.[34,35] The desorption of α (β) oxygen from a perovskite oxide is associated with changes of the valences of B-site ions and the formation of oxygen vacancies. Detailed analyses of the oxygen desorption (or absorption) behavior have already been described.[36,4] As shown in Figure 5, all samples except $Sr_{1.1}Co_{0.8}Fe_{0.2}O_{3-\delta}$, exhibit two kinds of characteristic desorption peaks (α/β-oxygen), with one at low temperature and the other at high temperature in the range of 100–950°C. It is suspected that $Sr_{1.1}Co_{0.8}Fe_{0.2}O_{3-\delta}$ may have another oxygen desorption peak at a temperature far above 950°C, as well as the one in the low temperature range of 300–600°C. This is because O_2-TPD plots recorded for most defect perovskite-type oxides (e.g., $La_{1-x}Sr_xCo_{1-y}Fe_yO_{3-\delta}$) have been characterized by the appearance of two types of oxygen desorption peaks, α and β oxygen.[36] A close study of the α-oxygen desorption peaks at low temperature (300–600°C) shows overlapping α-oxygen desorption peaks. The two α-oxygen peaks then split (or become more obvious) with the decrease of Sr concentrations for the series of $Sr_{1+x}Co_{0.8}Fe_{0.2}O_3$ ($-0.2 \leq x \leq 0.1$) oxides. Also, between the double α-oxygen peaks for each sample, the first one may result from the reduction of Co^{4+} to Co^{3+}, and the second from the reduction of Fe^{4+} to Fe^{3+}, because Fe^{3+} is more easily oxidized to Fe^{4+} than Co^{3+} to Co^{4+} for the perovskite-type $La_{1-x}A_xCo_{1-y}Fe_yO_{3-\delta}$·(A = Sr, Ba, Ca) oxides.[37] No matter how the synergetic effect of the B-site ions influences the O_2-TPD patterns of the $Sr_{1+x}Co_{0.8}Fe_{0.2}O_3$ ($-0.2 \leq x \leq 0.1$) oxides, the area of the α-oxygen desorption peaks of $Sr_{0.95}Co_{0.8}Fe_{0.2}O_3$ at the low temperature is the
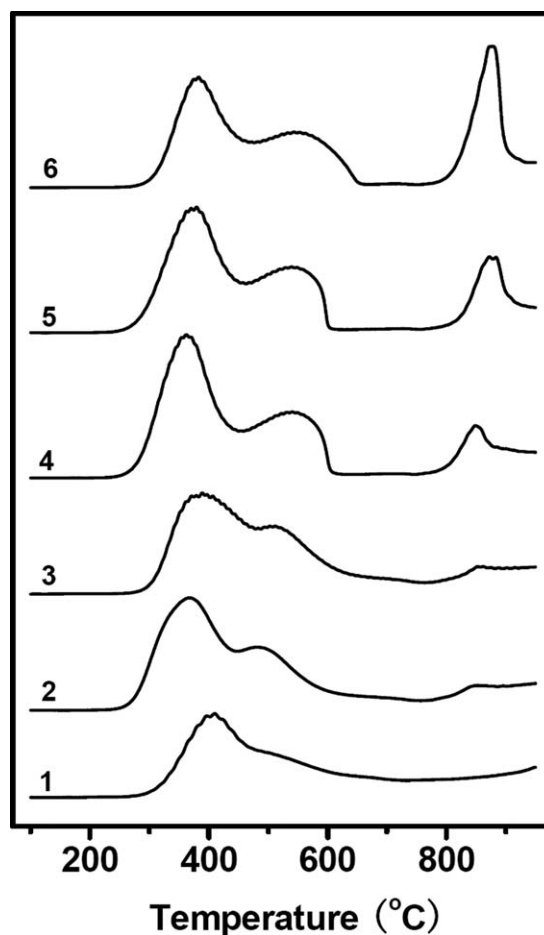

Figure 5. O_2-TPD profiles of the $Sr_{1+x}Co_{0.8}Fe_{0.2}O_{3-\delta}$ ($-0.2 \leq x \leq 0.1$) oxides in the temperature range of 100–950°C.

1. $Sr_{1.1}Co_{0.8}Fe_{0.2}O_{3-\delta}$, 2. $Sr_{1.05}Co_{0.8}Fe_{0.2}O_{3-\delta}$, 3. $Sr_{1.0}Co_{0.8}Fe_{0.2}O_{3-\delta}$, 4. $Sr_{0.95}Co_{0.8}Fe_{0.2}O_{3-\delta}$, 5. $Sr_{0.9}Co_{0.8}Fe_{0.2}O_{3-\delta}$, 6. $Sr_{0.8}Co_{0.8}Fe_{0.2}O_{3-\delta}$.

largest, followed by the oxides with $x = -0.1$ and then $x = 0.0$. As indicated in Table 1, the sequence of the amounts of the α-oxygen desorbed (or the areas of the α-oxygen desorption peaks) in the low temperature range of 300–600°C is consistent with that of the oxygen absorption capacities at $T = 500$°C (or 550°C). In addition, it is interesting to discover that the amounts of β-oxygen desorbed increase with the decrease of the concentrations of A-site ions for the $Sr_{1+x}Co_{0.8}Fe_{0.2}O_3$ ($-0.2 \leq x \leq 0.1$) oxides in the high temperature range of 750–950°C. In other words, the amounts of oxygen desorbed at the high temperature are also influenced by the stoichiometry of the A-site ions, which may be very useful for high temperature oxygen permeable membranes.

The long-term stability of an absorbent was investigated on a fixed-bed apparatus in our laboratory. $Sr_{0.9}Co_{0.8}Fe_{0.2}O_3$, which has a relatively large oxygen absorption capacity and high oxygen desorption rate at $T = 500$°C (or 550°C), was selected for the stability testing. The oxide showed an oxygen absorption capacity of 0.319 mmol/g at 500°C and 0.368 mmol/g at 550°C during the cycling process. As shown in Figure 6, it indicates that the average mole fraction
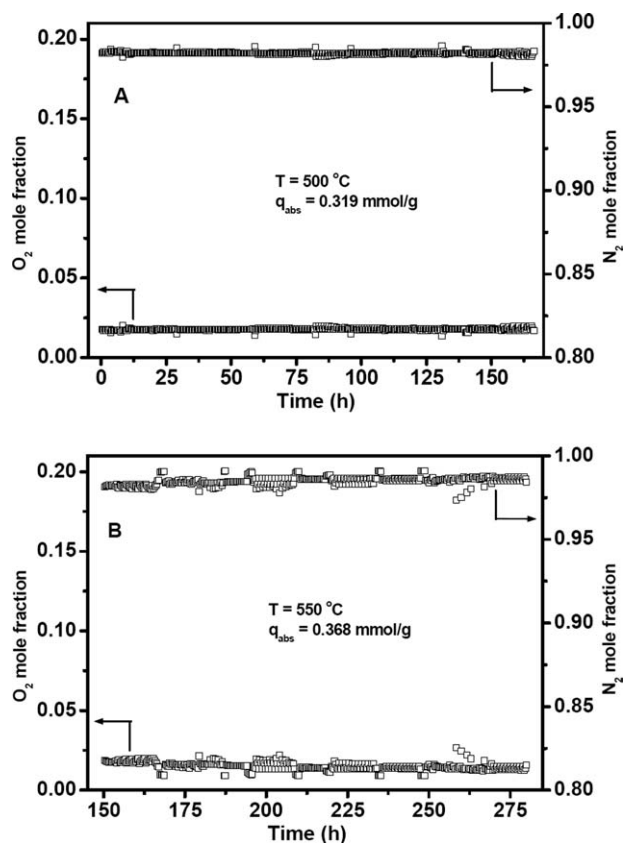
Figure 6. Long-term stability experiment of the Sr$_{0.9}$Co$_{0.8}$Fe$_{0.2}$O$_{3-\delta}$ oxide at (A) T = 500°C and (B) T = 550°C.

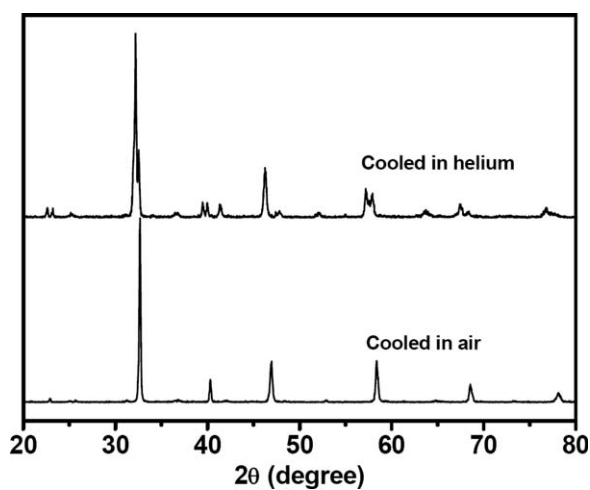**Figure 7. XRD patterns of the Sr$_{0.9}$Co$_{0.8}$Fe$_{0.2}$O$_{3-\delta}$ oxide after the long-term stability experiment shown in Figure 6.**

of oxygen is only about 1.6% and that of nitrogen reaches 98.4% in the effluent from the oxygen absorption bed. Over 280 h or 1120 cycles of oxygen desorption and absorption, the mole fractions of oxygen and nitrogen remain constant throughout, which suggests that the long-term stability and the cyclic properties of Sr$_{0.9}$Co$_{0.8}$Fe$_{0.2}$O$_3$ are excellent. Moreover, the oxide does not suffer fracture or pulverization after the long-term experiment, which further confirms its very good stability. Simply considering their excellent stability and cyclic properties, perovskite-type oxides used as oxygen absorbents would be a good choice among their
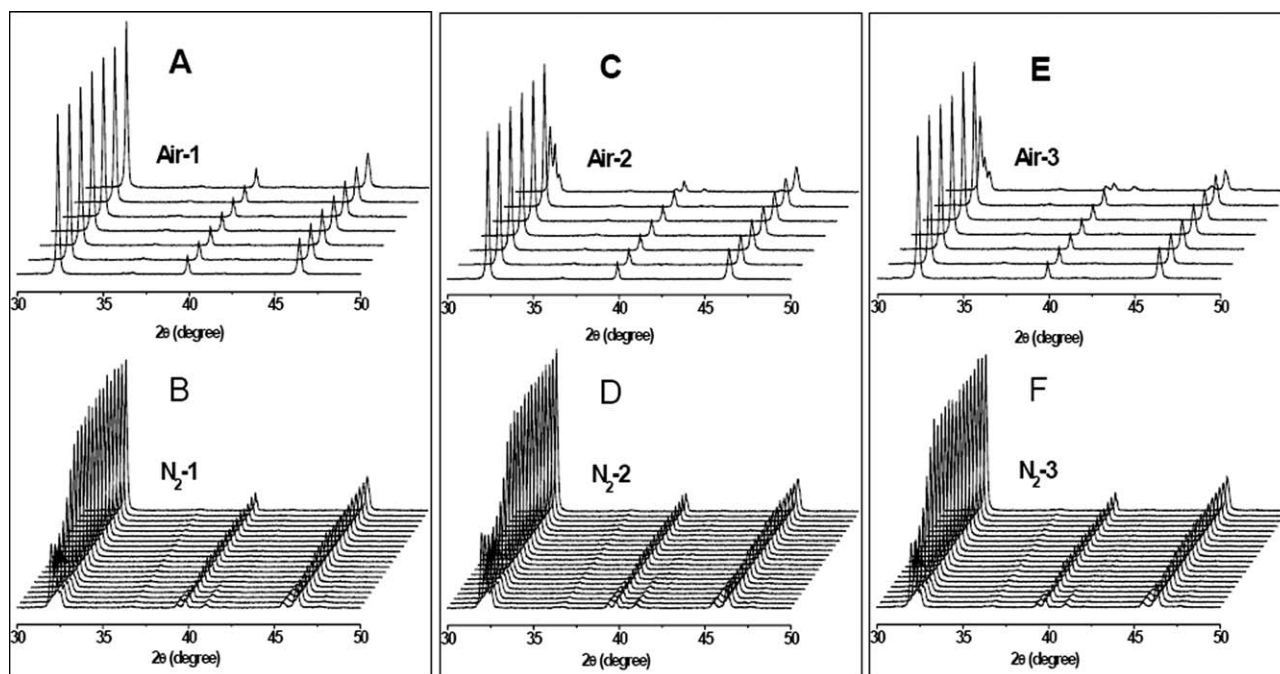

Figure 8. Patterns of high-temperature in-situ XRD at 500°C for Sr$_{0.9}$Co$_{0.8}$Fe$_{0.2}$O$_{3-\delta}$.

A/B are the oxygen absorption/desorption processes in the first cycle, C/D the processes in the second cycle and E/F the processes in the third cycle.

numerous applications. In addition, the good cycling stability of the absorbent is evidenced by the following XRD patterns.

The XRD patterns in Figure 7 show the structures of $Sr_{0.9}Co_{0.8}Fe_{0.2}O_3$ after the long-term stability experiment. It is clear that one sample retains a cubic perovskite structure, and the other has a brownmillerite-type structure. The upper XRD pattern, with the brownmillerite-type structure, is taken from the oxide cooled in helium atmosphere after 1120 cycles; the lower pattern, with the cubic perovskite structure, is of the oxide cooled in synthesized air. In other words, the upper XRD pattern represents the structure of the oxide which has been regenerated in the atmosphere with low oxygen partial pressure, while the lower pattern represents the oxide that has been saturated by air in oxidizing surroundings. In addition, the XRD pattern of the oxide cooled in helium suggests that $Sr_{0.9}Co_{0.8}Fe_{0.2}O_3$ undergoes a phase transition from the oxygen vacancy disordered structure (perovskite type) to the oxygen vacancy ordered structure (brownmillerite type) during the oxygen desorption process at $T = 550°C$. However, when the sample was re-exposed to air at the same temperature, it recovers to the perovskite structure exhibiting as the fresh one. In this way, the two patterns in Figure 7 provide a sound explanation why the oxygen absorption and desorption of $Sr_{0.9}Co_{0.8}Fe_{0.2}O_3$ shows high stability over many cycles, as shown in Figure 6.

To understand how the phase transitions occur and whether the reversibility of these phase transitions during the oxygen absorption/desorption cycles is good, the oxide $Sr_{0.9}Co_{0.8}Fe_{0.2}O_3$ was characterized by high temperature in situ XRD. In Figure 8, picture A shows the XRD patterns of $Sr_{0.9}Co_{0.8}Fe_{0.2}O_3$ originally exposed to synthesized air at $500°C$ for about 30 min, and picture B is the XRD patterns of the oxide which undergoes oxygen desorption in pure nitrogen for the first time. The oxide then absorbs and desorbs oxygen in the second cycle (pictures C and D), and then the third cycle (pictures E and F). From the six pictures, it is clear that $Sr_{0.9}Co_{0.8}Fe_{0.2}O_3$ exhibits a good reversibility between the structure with disordered oxygen vacancies (perovskite type) and the one with ordered oxygen vacancies (brownmillerite type) during the oxygen absorption and desorption cycles. Furthermore, as shown in Figure 8, impurities (CoO_x/FeO_x) retain the identical structures during all the oxygen absorption and desorption processes, and so their function might only be a catalyst to enhance the rates of oxygen absorption and desorption. For the second and third cycles in Figure 8, the main phase of $Sr_{0.9}Co_{0.8}Fe_{0.2}O_3$ recovers to the perovskite structure for the third sampling during the oxygen absorption processes, while it reverts to the brownmillerite structure from the perovskite structure for the 15 sampling during the oxygen desorption processes. This confirms our former work showing that the oxygen absorption process is faster than the oxygen desorption process.[19] In conclusion, the patterns of the in situ XRD, which have verified the result shown in Figure 7, suggest that $Sr_{0.9}Co_{0.8}Fe_{0.2}O_3$ has good long-term stability for oxygen absorption and desorption.

Conclusions

Perovskite-type oxides with an oxygen deficient structure, exhibited many advantages, such as large oxygen absorption capacities and an infinite selectivity for oxygen. In this article, the oxygen absorption and desorption properties of $Sr_{1+x}Co_{0.8}Fe_{0.2}O_3$ ($-0.2 \leq x \leq 0.1$) oxides were studied in the temperature range of 450–600°C. It was interesting to found that the A-site ion deficiency or excess of the perovskite oxide $SrCo_{0.8}Fe_{0.2}O_3$ resulted in larger oxygen absorption capacities and/or higher oxygen desorption rates than that with A-site ion stoichiometry. The CoO_x (FeO_x) oxides emerged in the A-site ion deficient $Sr_{0.9}Co_{0.8}Fe_{0.2}O_3$ and $Sr_{0.8}Co_{0.8}Fe_{0.2}O_3$ oxides could accelerate the oxygen desorption from the absorbents. The O_2-TPD experiment showed that the sequence of the amounts of α-oxygen was consistent with that of the oxygen absorption capacities measured on the fixed-bed equipment at 500 and 550°C. The oxygen desorption processes fit well with the pseudo-second-order kinetics model. The long-term stability testing of $Sr_{0.9}Co_{0.8}Fe_{0.2}O_3$ for 280 h (equivalent to 1120 cycles) indicated that perovskite-type oxides used as oxygen absorbents for oxygen separation will be another choice, besides the uses as dense oxygen permeable membranes and cathode materials for SOFCs. In addition, XRD patterns of $Sr_{0.9}Co_{0.8}Fe_{0.2}O_3$ further verified its excellent stability and reproducible behavior, with the cyclic processes of oxygen absorption and desorption taking place between the perovskite structure with disordered oxygen vacancies and the brownmillerite structure with ordered oxygen vacancies.

Literature Cited

1. Qiu L, Lee TH, Liu LM, Yang YL, Jacobson AJ. Oxygen permeation studies of $SrCo_{0.8}Fe_{0.2}O_{3-\delta}$. Solid State Ionics. 1995;76:321–329.
2. Shao ZP, Xiong GX, Tong JH, Dong H, Yang WS. Ba effect in doped $Sr(Co_{0.8}Fe_{0.2})O_{3-\delta}$ on the phase structure and oxygen permeation properties of the dense ceramic membranes. Sep Purif Technol. 2001;25:419–429.
3. Li QM, Zhu XF, He YF, Yang WS. Partial oxidation of methane in $BaCe_{0.1}Co_{0.4}Fe_{0.5}O_{3-\delta}$ membrane reactor. Catal Today. 2010;149:185–190.
4. Yamazoe N, Teraoka Y. Oxidation catalysis of perovskites-relationships to bulk structure and composition (valency, defect, etc.). Catal Today. 1990;8:175–199.
5. Zhang HZ, Yang WS. Highly efficient electrocatalysts for oxygen reduction reaction. Chem Commun. 2007;4215–4217.
6. Shao ZP, Haile SM. A high-performance cathode for the next generation of solid-oxide fuel cells. Nature. 2004;431:170–173.
7. Bouwmeester HJM, Kruidhof H, Burggraaf AJ. Importance of the surface exchange kinetics as rate limiting step in oxygen permeation through mixed-conducting oxides. Solid State Ionics. 1994;72:185–194.
8. Zhu XF, Yang WS. Composite membrane based on ionic conductor and mixed conductor for oxygen permeation. AIChE J. 2008;54:665–672.
9. Kovalevsky AV, Kharton VV, Tikhonovich VN, Naumovich EN, Tonoyan AA, Reut OP, Boginsky LS. Oxygen permeation through $Sr(Ln)CoO_{3-\delta}$ (Ln = La, Nd, Sm, Gd) ceramic membranes. Mate Sci Eng, B. 1998;52:105–116.
10. Lomakov MV, Istomin SY, Abakumov AM, Van Tendeloo G, Antipov EV. Synthesis and characterization of oxygen-deficient oxides $BaCo_{1-x}Y_xO_{3-y}$, x = 0.15, 0.25 and 0.33, with the perovskite structure. Solid State Ionics. 2008;179:1885–1889.

11. Lin YS, MacLean DL, Zeng YX. High-Temperature Adsorption Process. US Patent. 6,059,858, 2000.
12. Yang ZH, Lin YS, Zeng Y. High-temperature sorption process for air separation and oxygen removal. *Ind Eng Chem Res*. 2002;41: 2775–2784.
13. Kusaba H, Sakai G, Shimanoe K, Yamazoe N, Miura N. Temperature-swing based oxygen enrichment by using perovskite-type oxides. *J Mater Sci Lett*. 2002;21:407–409.
14. Karppinen M, Yamauchi H, Otani S, Fujita T, Motohashi T, Huang YH, Valkeapaa M, Fjellvag H. Oxygen nonstoichiometry in $YBaCo_4O_{7+\delta}$: large low-temperature oxygen absorption/desorption capability. *Chem Mater*. 2006;18:490–494.
15. Motohashi T, Kadota S, Fjellvag H, Karppinen M, Yamauchi H. Uncommon oxygen intake/release capability of layered cobalt oxides, $REBaCo_4O_{7+\delta}$: Novel oxygen-storage materials. *Mater Sci Eng, B*. 2008;148:196–198.
16. Kadota S, Karppinen M, Motohashi T, Yamauchi H. R-site substitution effect on the oxygen-storage capability of $RBaCo_4O_{7+\delta}$. *Chem Mat*. 2008;20:6378–6381.
17. Guntuka S, Banerjee S, Farooq S, Srinivasan MP. A- and B-site substituted lanthanum cobaltite perovskite as high temperature oxygen sorbent. 1. Thermogravimetric analysis of equilibrium and kinetics. *Ind Eng Chem Res*. 2008;47:154–162.
18. Guntuka S, Farooq S, Rajendran A. A- and B-Site substituted lanthanum cobaltite perovskite as high temperature oxygen sorbent. 2. Column dynamics study. *Ind Eng Chem Res*. 2008;47:163–170.
19. He YF, Zhu XF, Li QM, Yang WS. Perovskite oxide absorbents for oxygen separation. *AIChE J*. 2009;55:3125–3133.
20. Zhu XF, Sun SM, He YF, Cong Y, Yang WS. New concept on air separation. *J Membr Sci*. 2008;323:221–224.
21. Kostgloudis GC, Ftikos C. Properties of A-site-deficient $La_{0.6}Sr_{0.4-}Co_{0.2}Fe_{0.8}O_{3-\delta}$-based perovskite oxides. *Solid State Ionics*. 1999;126: 143–151.
22. Hansen KK, Hansen KV. A-site deficient $(La_{0.6}Sr_{0.4})_{1-s}Fe_{0.8}Co_{0.2}O_{3-\delta}$ perovskites as SOFC cathodes. *Solid State Ionics*. 2007;178: 1379–1384.
23. Kharton VV, Viskup AP, Naumovich EN, Tonoyan AA, Reut OP. Oxygen ionic transport in A-site-deficient perovskites $La(Pb)FeO_3$. *Mater Res Bull*. 1998;33:1087–1093.
24. Poulsen FW. Method for calculating ionic and electronic defect concentrations in proton containing perovskites. *J Solid State Electrochem*. 1999;143:115–121.
25. Waller D, Lane JA, Kilner JA, Steele BCH. The effect of thermal treatment on the resistance of LSCF electrodes on gadolinia doped ceria electrolytes. *Solid State Ionics*. 1996;86–88:767–772.
26. Ge L, Zhou W, Ran R, Liu SM, Shao ZP, Jin WQ, Xu NP. Properties and performance of A-site deficient $(Ba_{0.5}Sr_{0.5})_{1-x}Co_{0.8}Fe_{0.2}O_{3-\delta}$ for oxygen permeating membrane. *J Memb Sci*. 2007;306:318–328.
27. Ge L, Ran R, Zhang K, Liu SM, Shao ZP. Oxygen selective membranes based on B-site cation-deficient $(Ba_{0.5}Sr_{0.5})(Co_{0.8}Fe_{0.2})_yO_{3-\delta}$ perovskite with improved operational stability. *J Membr Sci*. 2008; 318:182–190.
28. Zhou W, Ran R, Shao ZP, Zhuang W, Jia J, Gu HX, Jin WQ, Xu NP. Barium- and strontium-enriched $(Ba_{0.5}Sr_{0.5})_{1+x}Co_{0.8}Fe_{0.2}O_{3-\delta}$ oxides as high-performance cathodes for intermediate-temperature solid-oxide fuel cells. *Acta Mater*. 2008;56:2687–2698.
29. Shao ZP, Yang WS, Cong Y, Dong H, Tong JH, Xiong GX. Investigation of the permeation behavior and stability of a $Ba_{0.5}Sr_{0.5}Co_{0.8}Fe_{0.2}O_{3-\delta}$ oxygen membrane. *J Membr Sci*. 2000;172: 177–188.
30. Jansson J. Low-temperature CO oxidation over Co_3O_4/Al_2O_3. *J Catal*. 2000;194:55–60.
31. Hao HS, Zheng L, Wang YF, Liu SJ, Hu X. Thermogravimetric study on oxygen adsorption/desorption properties of double perovskite structure oxides $REBaCo_2O_{5+\delta}$ (RE = Pr, Gd, Y). *J Rare Earths*. 2007;25:275–281.
32. Marczewski AW. Kinetics and equilibrium of adsorption of organic solutes on mesoporous carbons. *Appl Surf Sci*. 2007;253:5818–5826.
33. Yin QH, Kniep J, Lin YS. Oxygen sorption and desorption properties of Sr–Co–Fe oxide. *Chem Eng Sci*. 2008;63:2211–2218.
34. Yamazoe N, Teraoka Y, Seiyama T. TPD and XPS study on thermal behavior of absorbed oxygen in $La_{1-x}Sr_xCoO_{3-\delta}$. *Chem Lett*. 1981;1767–1770.
35. Teraoka Y, Zhang HM, Yamazoe N. Oxygen-sorption properties of defect perovskite-type $La_{1-x}Sr_xCo_{1-y}Fe_yO_{3-\delta}$. *Chem Lett*. 1985; 1367–1370.
36. Teraoka Y, Yoshimatsu M, Yamazoe N, Seiyama T. Oxygen-sorptive properties and defect structure of perovskite-type oxides. *Chem Lett*. 1984;893–896.
37. Stevenson JW, Armstrong TR, Carneim RD, Pederson LR, Weber WJ. Electrochemical properties of mixed conducting perovskites $La_{1-x}M_xCo_{1-y}Fe_yO_{3-\delta}$ (M = Sr, Ba, Ca). *J Electrochem Soc*. 1996;143:2722–2729.